

Supporting Information

Single yttrium sites on carbon-coated TiO₂ for efficient electrocatalytic N₂ reduction

Lianghao Yang,^a Changhyeok Choi,^b Song Hong,^c Zhiming Liu,^a Zhenqing Zhao,^a Mengmeng Yang,^a Huidong Shen,^a Alex W. Robertson,^d Hao Zhang,^e Tsz Woon Benedict Lo,^e Yousung Jung,^{b,*} Zhenyu Sun^{a,*}

^a State Key Laboratory of Organic–Inorganic Composites, College of Chemical Engineering, Beijing University of Chemical Technology, Beijing 100029, P. R. China. E-mail: sunzy@mail.buct.edu.cn

^b Department of Chemical and Biomolecular Engineering, Korea Advanced Institute of Science and Technology (KAIST), Daejeon 34141, Republic of Korea

^c Analysis Technology R&D Center, Beijing University of Chemical Technology, P. R. China

^d Department of Materials, University of Oxford, Oxford OX1 3PH, U. K.

^e Department of Applied Biology and Chemical Technology, The Hong Kong Polytechnic University, Hong Kong, P. R. China

Experimental

Chemicals and reagents

All chemicals used in this work were of analytical grade and used without further treatments. Ammonium chloride, sodium hydroxide, salicylic acid, sodium citrate, sodium hypochlorite, and sodium nitroferrocyanide were obtained from Sigma-Aldrich Chemical Reagent Co. HCl (37.0%) was provided by Beijing Chemical Works. Yttrium chloride was purchased from Macklin. Glucose was acquired from Aladdin. Titanium isopropoxide was purchased from Aladdin. Carbon black (Vulcan XC-72) was purchased from Fuel Cell Store. Nafion solution (5.0 wt%) was acquired from Sigma-Aldrich and Nafion membranes were provided by Alfa Aesar. Deionized water was used in all experiments. ¹⁴N₂ gas (99.999% purity) and argon gas (99.999% purity) were obtained from Beijing Haipu Gas Co., Ltd (<http://151999.71ab.com/>). ¹⁴N₂ gas (99.9999% purity) was provided by Hycegas Co., Ltd (<http://www.hycegas.com/>). ¹⁵N₂ gas (99.0% ¹⁵N≡¹⁵N) was purchased from Guangzhou Yigas Gases Co., Ltd (<http://www.yigas.cn/>).

Catalyst preparation

Synthesis of Y-TiO₂-C

Typically, 1.05 g of glucose, a specific amount of yttrium chloride (Y loading: 0–3 wt%), and 0.5 g of HCl (37%) solution were first added in 40 mL of deionized water under magnetic stirring followed by dropwise addition of 1.05 g of titanium isopropoxide. The mixture was subjected to magnetic stirring at ambient temperature for 2 h to allow complete homogenization. The mixture was then transferred to a 100 mL high-pressure steel reactor, which was subjected to heating at 180 °C for 18 h. The resultant precipitate was washed repeatedly by water and ethanol respectively, and then dried in an oven at 60 °C overnight. Subsequently, the obtained powder was annealed in a quartz-tube furnace at 900 °C for 2 h under argon atmosphere at a heating rate of 5 °C min⁻¹, which was then cooled to room temperature to yield Y-TiO₂-C.

The TiO₂-C composite (TiO₂-C) without Y, Y-TiO₂ without glucose, and TiO₂ without yttrium and glucose were also prepared by a similar process.

Characterization

X-ray powder diffraction (XRD) was performed with a D/MAX-RC diffractometer operated at 30 kV and 100 mA with Cu K α radiation. XPS experiments were carried out using Thermo Scientific ESCALAB 250Xi instrument. The instrument was equipped with an electron flood and scanning ion gun. All spectra were calibrated to the C 1s binding energy at 284.8 eV. High-angle annular dark field scanning TEM (HAADF-STEM) was conducted using a JEOL ARM200 microscope with 200 kV accelerating voltage. STEM samples were prepared by depositing a droplet of suspension onto a Cu grid coated with a Lacey Carbon film. Raman spectra were collected with a Renishaw in Via Raman microscope with a He/Ne Laser excitation at 532 nm (2.33 eV). Nitrogen adsorption/desorption measurements at 77 K were performed on a Micromeritics ASAP2460 to obtain pore properties such as the specific surface area, total pore volume, and pore size distribution. The sample was degassed at 200 °C for 1 h.

Purification of 99.9999% N₂ by SCR with NH₃

The SCR process was performed in a fixed-bed quartz flow reactor, which contained 100 mg of Ce_{0.1}Ti_{0.9}O₂ catalyst at atmospheric pressure. N₂ (99.9999%) at a flow rate of 25 sccm and 1.3% NH₃/N₂ at a flow rate of 2 sccm reacted over the catalyst surface

in the reactor at 300 °C, which ensured reduction of NO_x impurities in the original N₂ into N₂ and H₂O. The gas mixture after SCR flowed through two acid traps consisting of 17% H₃PO₄ solutions and further through an acid trap consisting of 20% H₂SO₄ solution to sufficiently adsorb NH₃ remaining before continuously fed into the cathodic compartment during the experiment. The influence of NH₃ remaining on determination of NH₃ yield rate was excluded by subtracting the amount of NH₄⁺ in the electrolyte over an equivalent period without running electrolysis.

Electrochemical measurements

Typically, 0.5 mg of catalysts were dispersed in 120 μL of isopropanol aqueous solution (IPA-to-H₂O volume ratio of 1:1) to form a homogeneous ink under bath ultrasonication for 1 h. The dispersion was then loaded onto a carbon paper electrode with an area of 1 x 1 cm² and dried under ambient conditions. Finally, 5 μL of a Nafion solution (1 wt%) was dropped on the carbon paper. Controlled potential electrolysis of N₂ was performed in an H-shape electrochemical cell with a Nafion 117 membrane to separate the working and counter electrode compartments. Before NRR tests, the Nafion membrane was pre-treated by heating in 5% H₂O₂ aqueous solution at 80 °C for 1 h and subsequently in 0.5 M H₂SO₄ at 80 °C for another 1 h. Toray Carbon fiber paper with a size of 1 cm × 1 cm was employed as working electrode. Pt wire and Ag/AgCl electrodes were used as counter electrode and reference electrode, respectively. The potentials were controlled by an electrochemical working station (CHI 660E, Shanghai CH Instruments Co., China). All potentials in this study were measured against the Ag/AgCl reference electrode (in 3 M aqueous KCl corresponding to an $E^{\circ}_{\text{Ag/AgCl}} = 0.205$ V) and converted to the RHE reference scale by

$$E (\text{vs. RHE}) = E (\text{vs. Ag/AgCl}) + 0.205 + 0.059 \times \text{pH} \quad (\text{Eq. S1})$$

Electrocatalytic fixation of N₂ was carried out at ambient temperatures and atmospheric pressure ($\text{N}_2 + 6\text{H}_2\text{O} + 6\text{e}^- \rightleftharpoons 2\text{NH}_3 + 6\text{OH}^-$). N₂ (99.999%) (Fig. S6a) or N₂ (99.9999%) (Fig. S6b) was purged into the electrolyte for at least 30 min to remove residual air in the reservoir, then controlled potential electrolysis was conducted at each potential for 60 min with N₂ flowing through the cell (the volume of electrolyte in either anode or cathode chamber is 30 mL). During the electrolysis, the electrolyte was agitated with a bar stirrer at a stirring rate of about 500 rpm. The flow rate of N₂ passed through the cell was regulated by a mass flow controller (Sevenstar Instrument). A flow

rate of 30 mL min⁻¹ was selected to ensure sufficient N₂ transport to the surface while excluding interference from gas bubbles striking the surface. We performed Y-TiO₂-C catalysts in N₂ experiments for at least three times, each with a new electrode.

Determination of ammonia

The concentration of produced ammonia was spectrophotometrically determined by the indophenol blue method.¹ In detail, 2 mL aliquot of the solution was removed from the electrochemical reaction vessel. Then, 2 mL of a 1 M NaOH solution containing 5 wt% salicylic acid and 5 wt% sodium citrate was added, followed by addition of 1 mL of 0.05 M NaClO and 0.2 mL of 1 wt% C₅FeN₆Na₂O (sodium nitroferricyanide) aqueous solution. After 2 h of incubation at room temperature, the absorption spectrum was measured using an ultraviolet-visible spectrophotometer. The formation of indophenol blue was determined based on the absorbance at a wavelength of 655 nm. The concentration-absorbance curves were calibrated using standard ammonia chloride solutions, as shown in Fig. S7, which contained the same concentrations of HCl as used in the electrolysis experiments. The measurements with the background solutions (no NH₃) were conducted for all experiments, and the background peak absorbance was subtracted from the measured peak absorbance of NRR experiments to estimate the NH₃ concentrations and the faradaic efficiencies.

The concentration of ammonia was also quantified by NMR spectroscopy on a Bruker AV 600-MHz system (Fig. S8). Specifically, 26 mL of the electrolyte solution extracted from the electrochemical cell after the NRR at -0.22 V (*vs.* RHE) was first concentrated to approximately 1.5 mL.² 500 μ L of the concentrated solution was then mixed with 50 μ L of DMSO-d₆ for ¹H NMR measurements.

Determination of hydrazine

The formation of hydrazine during electrolysis was examined by the method of Watt and Chrisp.³ A mixture of para-(dimethylamino) benzaldehyde (5.99 g), HCl (37.0%, 30 mL), and ethanol (300 mL) was used as a color reagent. To do calibration, a series of reference solutions were firstly prepared by pipetting suitable volumes of hydrazine hydrate-nitrogen 0.1 M HCl solution in colorimetric tubes. Then, 5 mL of diluted HCl electrolyte (pH 1) was prepared. Subsequently, 5 mL of the above prepared color reagent was mixed and stirred for 10 min at room temperature. Finally, the absorbance of the resulting solution was measured at 455 nm, and the yields of hydrazine were

estimated from a standard curve using 5 mL of residual electrolyte and 5 mL of color reagent.

Calculation of NH₃ faradaic efficiency (FE) and NH₃ yield rate

The FE was calculated from the charge consumed for NH₃ generation and the total charge passed through the electrode:

$$FE = (3F \times C_{\text{NH}_3} \times V)/Q \quad (\text{Eq. S2})$$

The yield rate of NH₃ can be estimated using the following equation:

$$\text{Yield rate} = (C_{\text{NH}_3} \times V)/(t \times m) \quad (\text{Eq. S3})$$

where F is the faraday constant (96,485 C mol⁻¹), C_{NH_3} is the measured NH₃ concentration, V is the volume of the electrolyte, Q is the total charge passed through the electrode, t is the electrolysis time (1 h), and m is the metal mass or the total mass of the catalyst. The reported NH₃ yield rate, NH₃ FE, and corresponding error bars were obtained based on the measurements of at least three separately prepared samples under the same conditions.

¹⁵N isotope labeling experiments

Isotope labeling test was conducted in ¹⁵N₂-saturated diluted hydrochloric acid electrolyte (pH 1, 40 mL). A ¹⁵N₂ gas first flowed through an acid trap consisting of 0.05 M H₂SO₄ solution before continuously fed into the cathodic compartment at a constant flow rate of 10 mL min⁻¹ during the experiment. After the electrolytic test for 6 h, the obtained ¹⁵NH₄⁺-contained electrolyte was analyzed by ¹H NMR spectroscopy (nuclear magnetic resonance, Bruker AV 600-MHz).

Density functional theory (DFT) calculations

DFT calculations have been employed to investigate various catalysts for NRR, such as transition metal surfaces,^{4,5} nitrides,^{6,7} oxides,^{8,9} sulfides,¹⁰ and single-atom catalysts.¹¹ All calculations were performed using spin-polarized density functional theory (DFT) implemented in the Vienna Ab initio Simulation Package (VASP) with projector-augmented wave pseudopotential (PAW).¹²⁻¹⁴ We used revised PBE (RPBE) functional developed by Norskov and coworkers.^{15,16} A cutoff energy was set to be 400 eV. The convergence criteria for the electronic energy difference and forces are 10⁻⁵ eV and 0.05 eV / Å, respectively.

We modelled two defective graphene as a support for a single Y atom: a carbon single-vacancy surrounded by three carbon atoms ($Y@C_3$) and a carbon double-vacancy surrounded by four carbon atoms ($Y@C_4$). A (2×1) supercell with four O-Ti-O layers of rutile $TiO_2(110)$ surface is chosen as a model system to construct TiO_2 . The bottom two layers were fixed at their optimized bulk positions, while other atoms are fully relaxed. A single Y atom embedded at TiO_2 ($Y@TiO_2$) is modelled by the rutile $TiO_2(110)$ surface where one of the surface Ti atom is substituted by Y atom. All slab models include more than 15 Å of vacuum in c-axis. The k-points were sampled using the $(2 \times 2 \times 1)$ and $(5 \times 4 \times 1)$ Monkhorst-Pack mesh¹⁷ for $Y@C_x$ and $Y@TiO_2$, respectively. All slab models are shown in Fig. 4a.

The computational hydrogen electrode model (CHE)¹⁸ was used to obtain the free energy profile for proton-coupled electron transfer step in NRR. In this model, the chemical potential of proton and electron pair is equal to the half of the chemical potential of 1 bar of $H_2(g)$ ($\mu(H^+ + e^-) = 0.5 \mu(H_2(g))$).

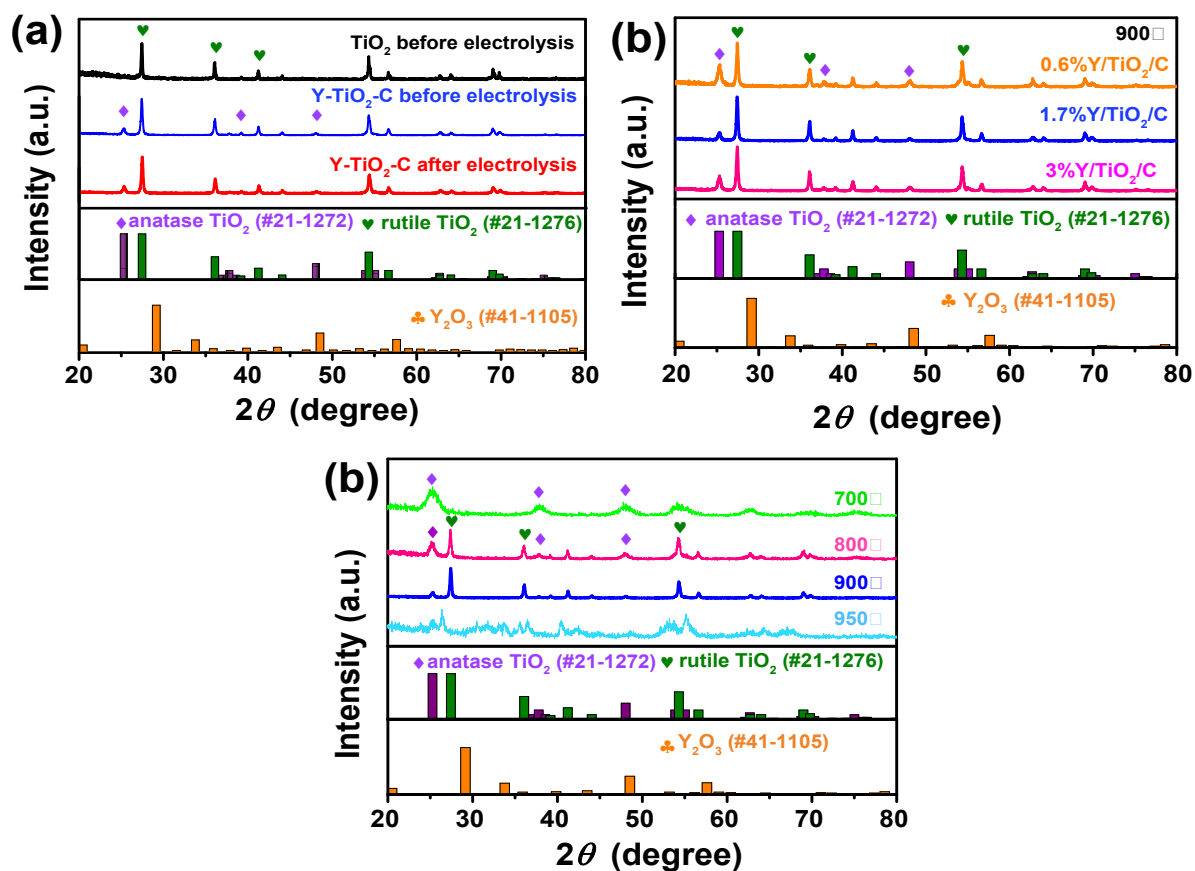


Fig. S1 XRD patterns of (a) pure TiO_2 , Y- TiO_2 -C (before electrolysis), and Y- TiO_2 -C (after electrolysis), (b) 0.6%Y- TiO_2 -C, 1.7%Y- TiO_2 -C, and 3%Y- TiO_2 -C, and (c) Y- TiO_2 -C samples obtained at 700, 800, 900, and 950 °C. The loading of Y for the samples in part b is 1.7 wt%.

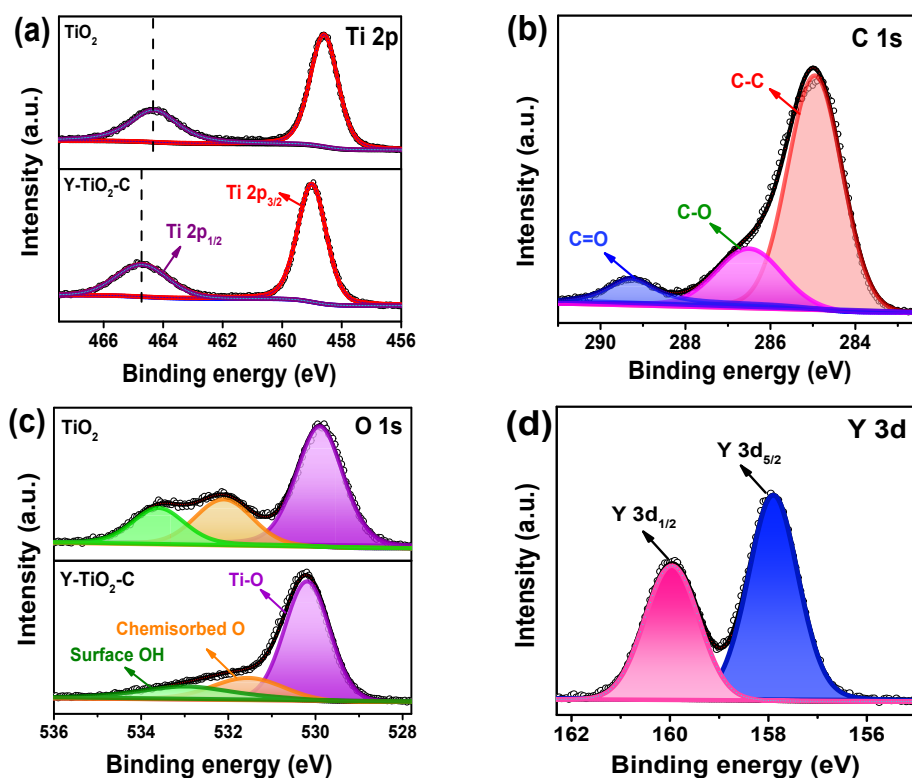


Fig. S2 (a) Ti 2p XPS spectra of pure TiO_2 and 1.7%Y- TiO_2 -C. (b) C 1s XPS spectrum of 1.7%Y- TiO_2 -C. (c) O 1s XPS spectra of pure TiO_2 and 1.7%Y- TiO_2 -C. (d) Y 3d XPS spectrum of Y- TiO_2 -C.

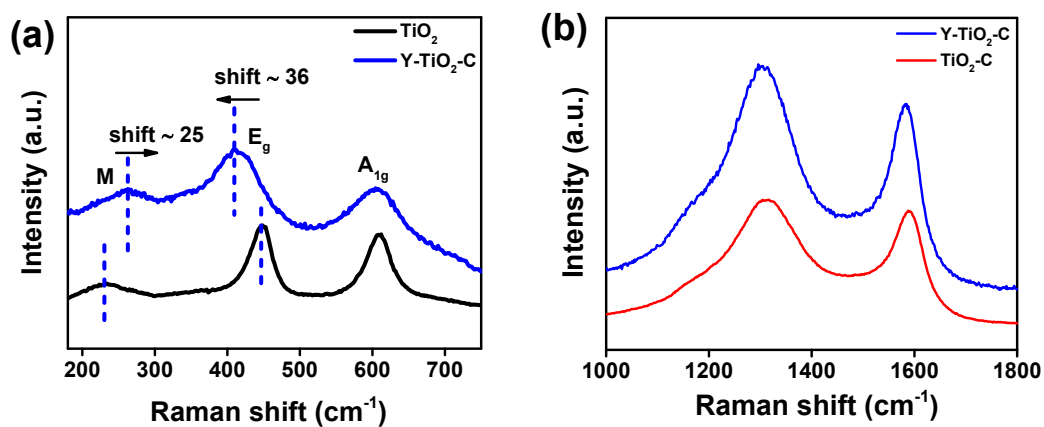


Fig. S3 (a) Raman spectra of TiO_2 and 1.7%Y- TiO_2 -C. (b) Raman spectra of TiO_2 -C and 1.7%Y- TiO_2 -C.

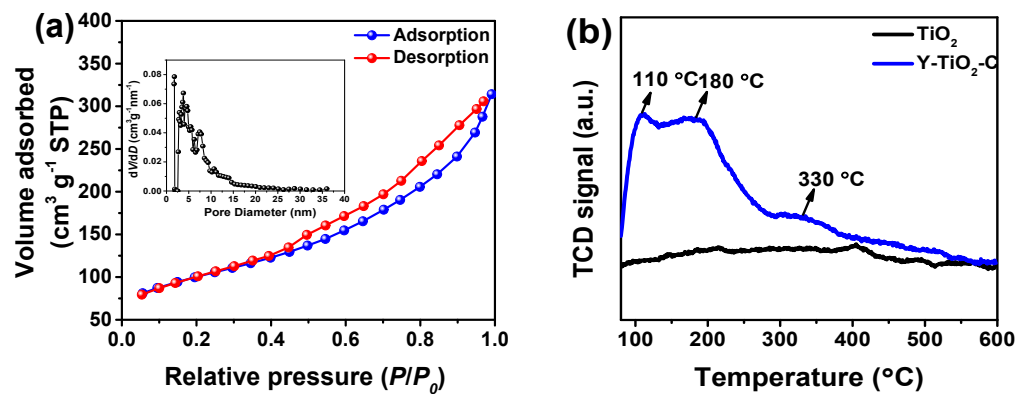


Fig. S4 (a) N_2 adsorption-desorption isotherms of 1.7%Y-TiO₂-C. The inset shows the pore size distribution of the sample. (b) N_2 -TPD profiles of TiO₂ and Y-TiO₂-C. The loading of Y in the Y-TiO₂-C samples is 1.7 wt%.

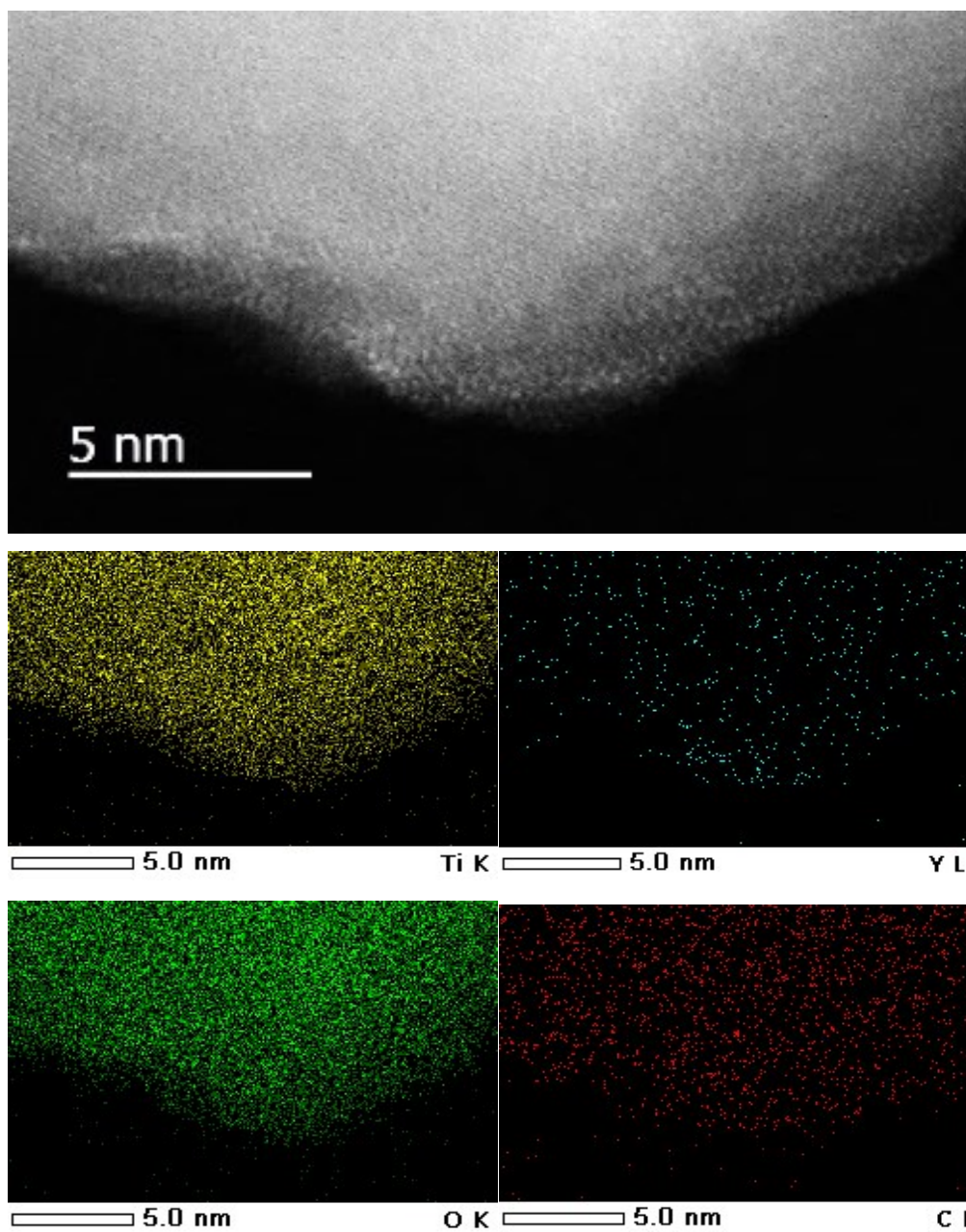


Fig. S5 HAADF-STEM image of 1.7%Y-TiO₂-C and corresponding EDS elemental maps of Ti, O, C, and Y. The brighter spots in the image are most likely single Y atoms.

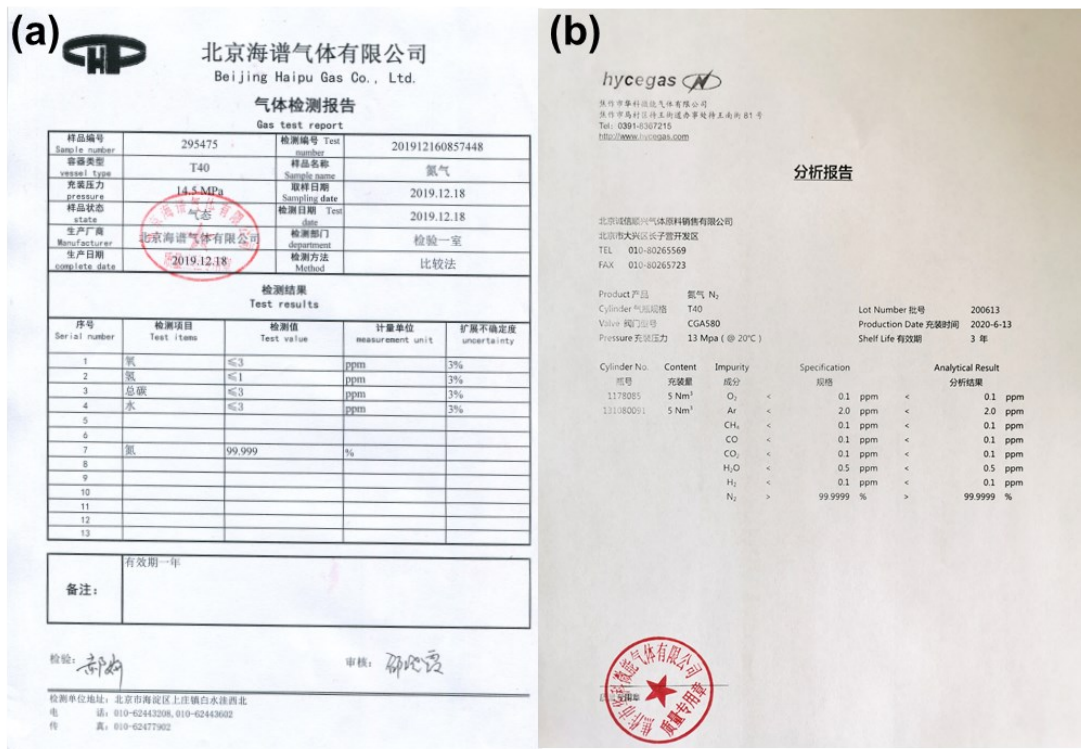


Fig. S6 Scanned certificates of (a) ¹⁴N₂ [99.999% purity, impurities containing O ≤ 3.0 ppm (vol.), H ≤ 1.0 ppm (vol.), C ≤ 3.0 ppm (vol.), and H₂O ≤ 3.0 ppm (vol.)] from Beijing Haipu Gas Co., Ltd. and (b) ¹⁴N₂ [99.9999% purity, impurities (CH₄ < 0.1 ppm (vol.), O₂ < 0.1 ppm (vol.), H₂ < 0.1 ppm (vol.), CO < 0.1 ppm (vol.), H₂O < 0.5 ppm (vol.), and CO₂ < 0.1 ppm (vol.))] from Hycegas Co., Ltd.

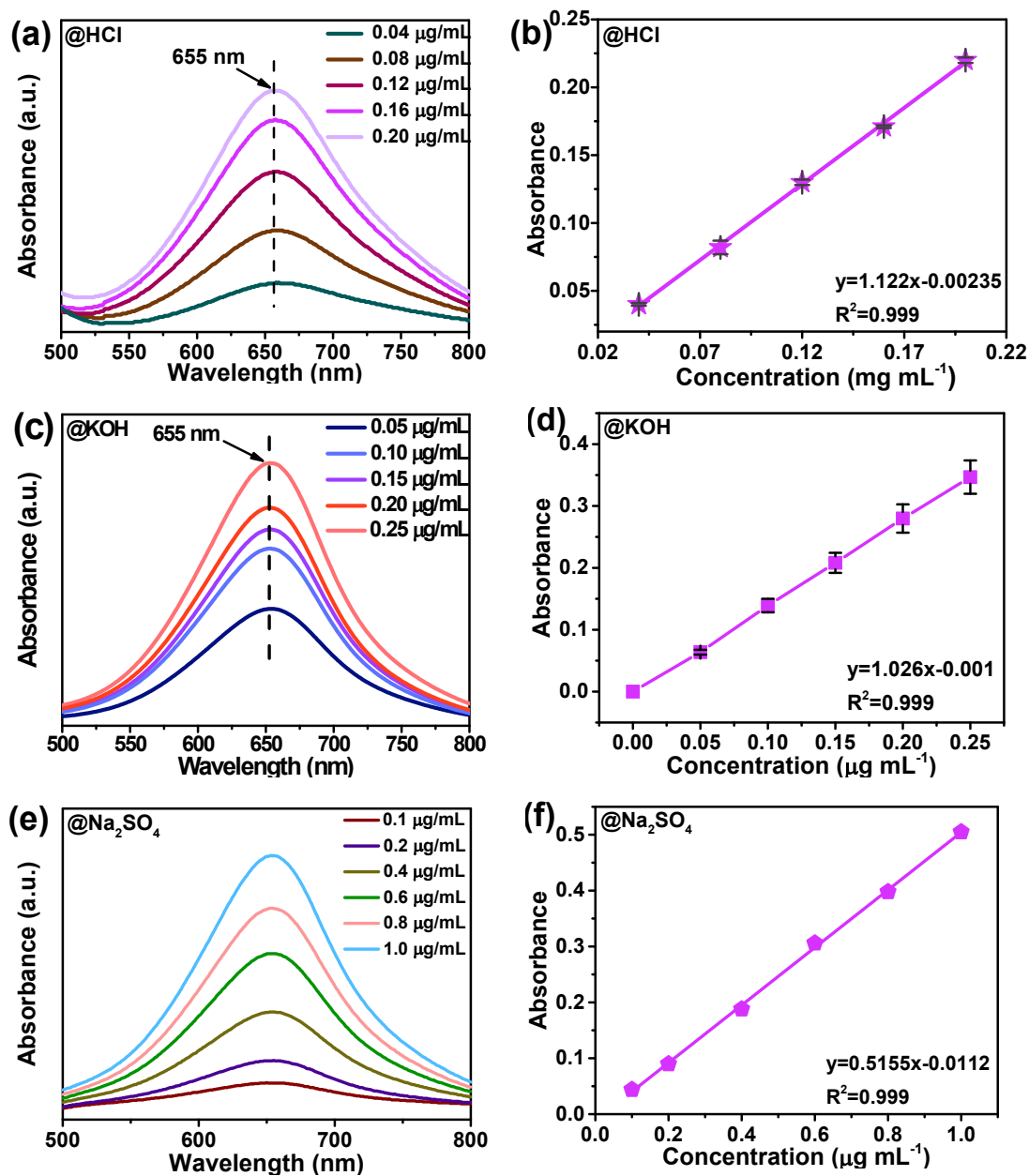


Fig. S7 UV-Vis curves of indophenol assays with NH_4^+ ions after incubated for 2 h at room temperature in (a) 0.1 M HCl, (c) 0.1 M KOH, and (e) 0.1 M Na_2SO_4 . The calibration curves used for estimation of NH_3 by NH_4^+ ion in (b) 0.1 M HCl, (d) 0.1 M KOH, and (f) 0.1 M Na_2SO_4 .

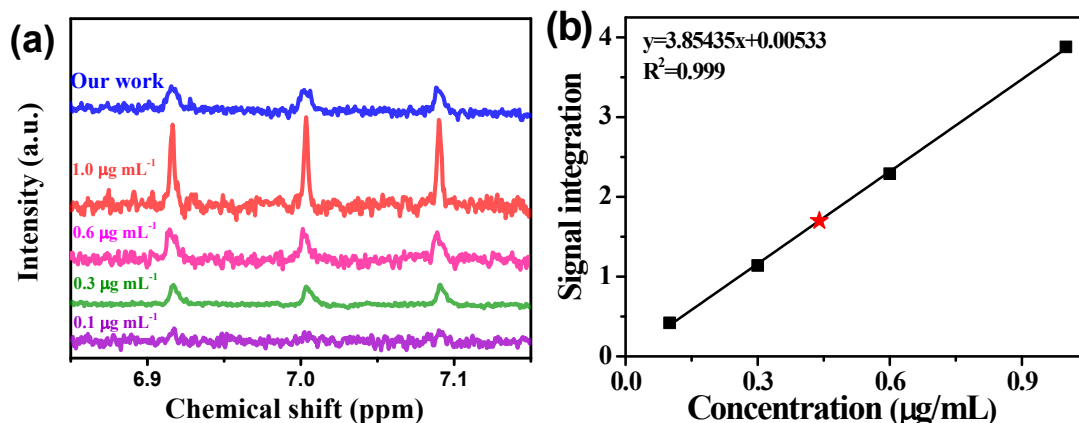


Fig. S8 (a) ¹H NMR spectra for standard NH₄⁺ solutions with concentrations of 0.1, 0.3, 0.6, 1.0 μg mL⁻¹, and the electrolyte after electrolysis at -0.22 V in N₂-saturated 0.1 M HCl. (b) Calibration curve of ¹H NMR signal for standard NH₄⁺ solutions with concentrations of 0.1, 0.3, 0.6, and 1.0 μg mL⁻¹ in 0.1 M HCl. The black line is the linear fitting of NMR signal integration value (versus NH₄⁺ ion concentration) with an R² value of 0.999. The red star indicates the concentration of NH₄⁺ in the electrolyte after 1 h of NRR at -0.22 V (vs. RHE) using the 1.7%Y-TiO₂-C.

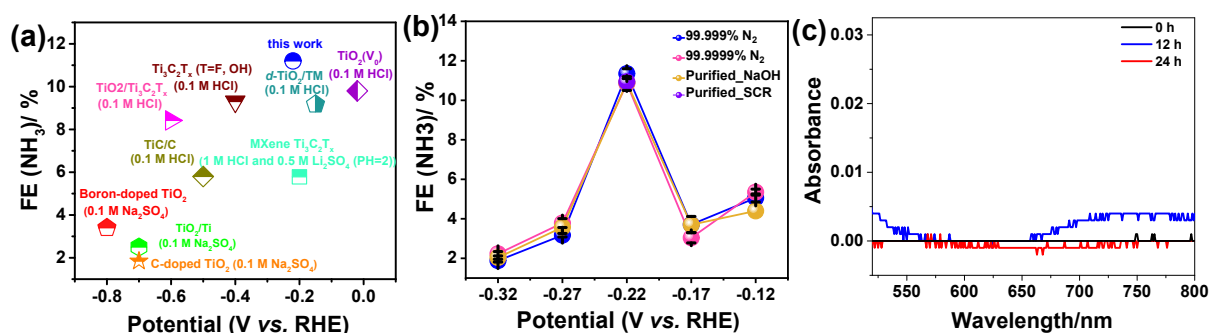


Fig. S9 (a) Comparisons of the maximum NH₃ FE of Y-TiO₂-C with other reported TiO₂-based electrocatalysts. (b) Comparisons of NH₃ FEs at different applied potentials over Y-TiO₂-C using a feed gas of 99.999% N₂, 99.9999% N₂, purified 99.9999% N₂ with 10 M NaOH (Purified_NaOH) or by SCR (Purified_SCR). (c) UV-Vis absorption spectra of the electrolytes exposed to the air for different times.

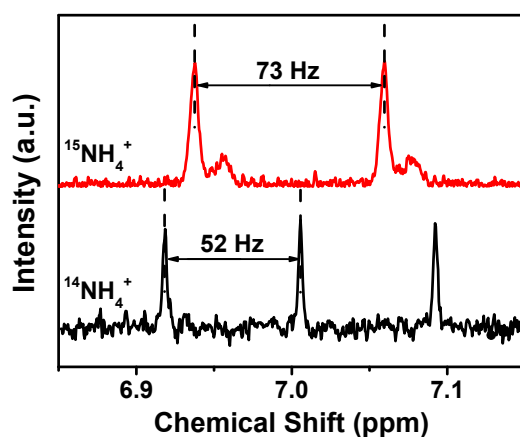


Fig. S10 ^1H NMR spectra of the electrolyte fed by $^{14}\text{N}_2$ or $^{15}\text{N}_2$ after the electrolytic reactions.

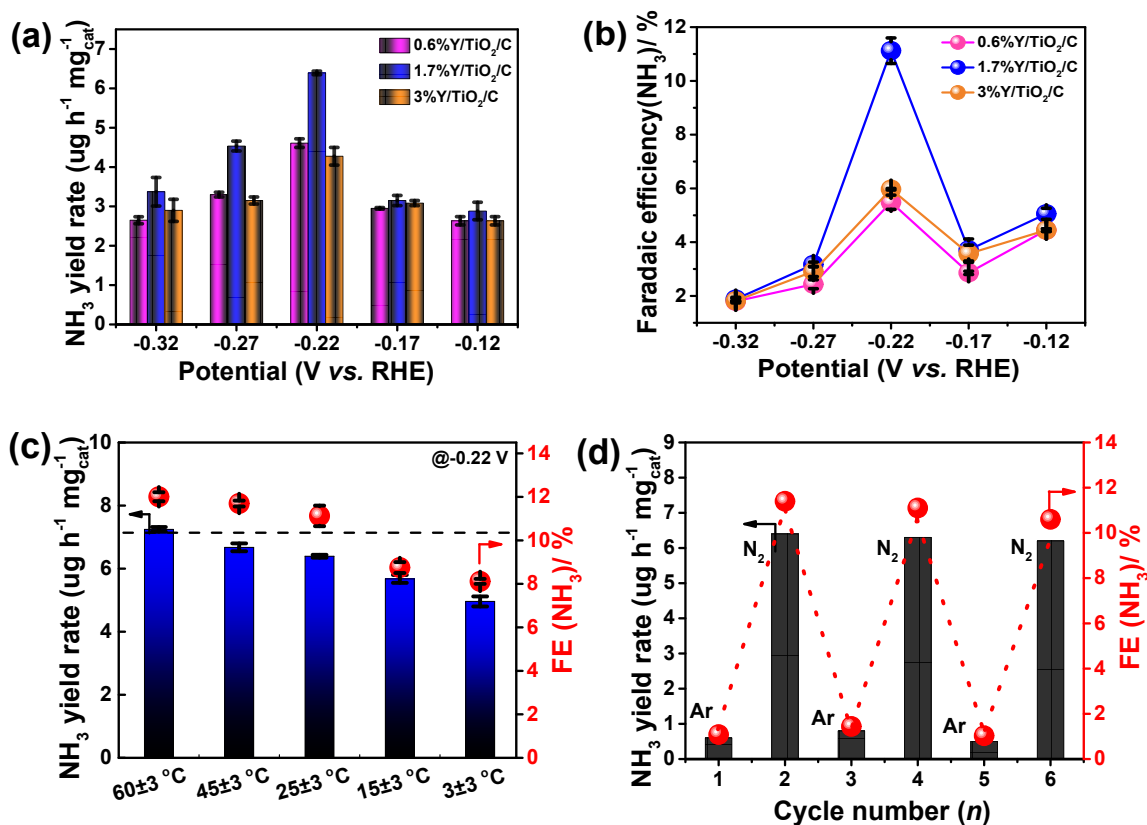


Fig. S11 (a) The yield rate and (b) *FE* for NH_3 formation at different applied potentials over 1.7%Y-TiO₂-C with varying Y loading contents. (c) The yield rate and *FE* for NH_3 formation versus NRR temperature at -0.22 V over 1.7%Y-TiO₂-C. (d) The NH_3 yield rate and *FE* with alternated Ar and N₂ cycles at -0.22 V over 1.7%Y-TiO₂-C.

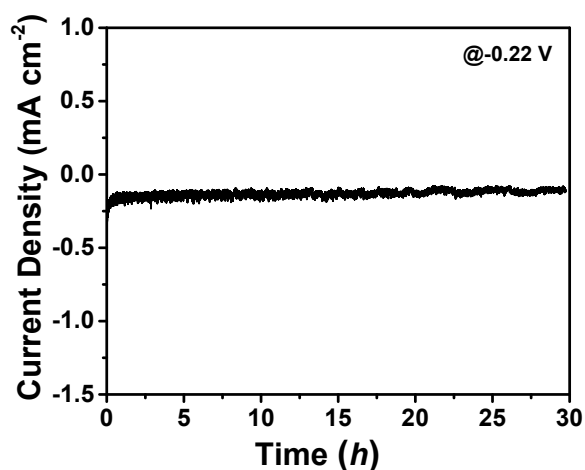


Fig. S12 Chronoamperometry measurements at -0.22 V over 1.7%Y-TiO₂-C.

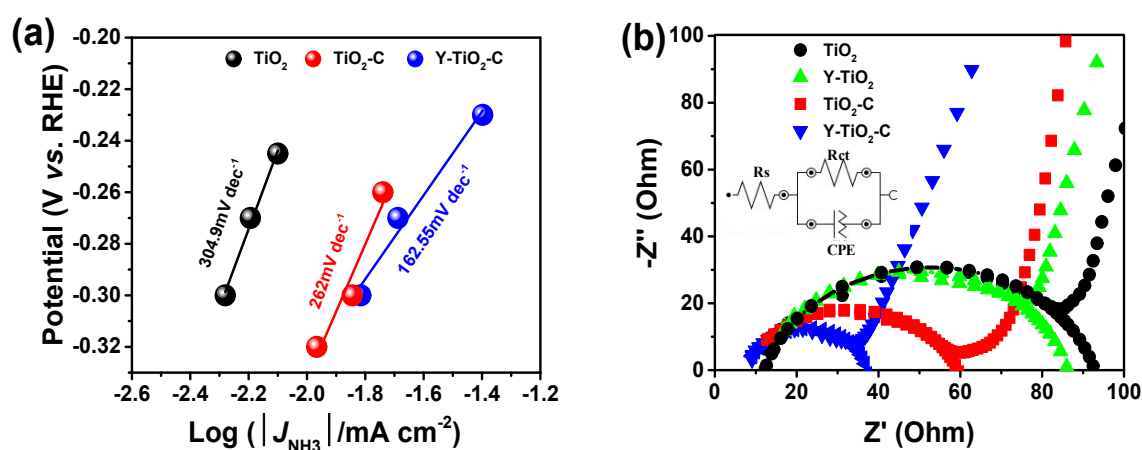


Fig. S13 (a) Tafel plots of NRR over Y-TiO₂-C, TiO₂-C, and TiO₂. (b) Nyquist profiles of Y-TiO₂-C, Y-TiO₂, TiO₂-C, and TiO₂.

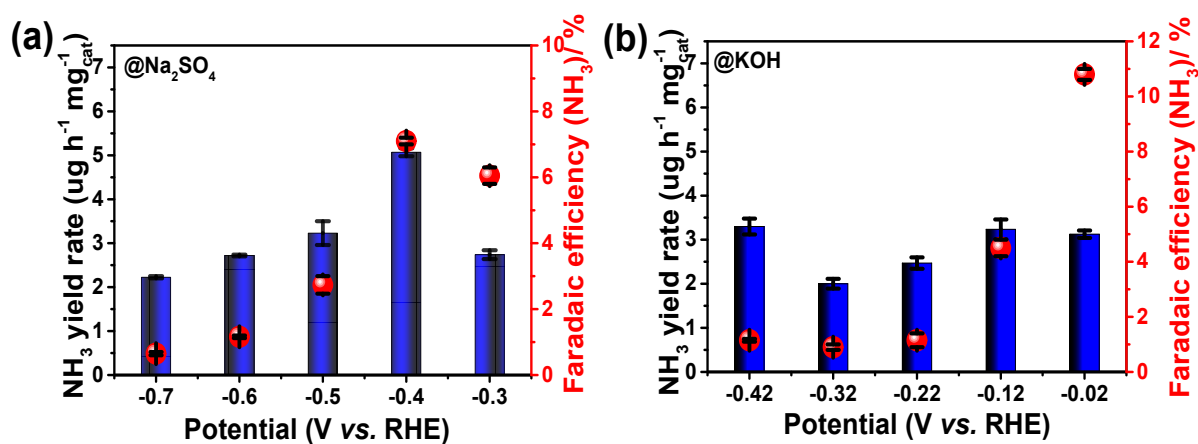


Fig. S14 The yield rates and *FEs* of NH₃ over 1.7%Y-TiO₂-C at different applied potentials in N₂-saturated (a) 0.1 M Na₂SO₄ and (b) 0.1 M KOH.

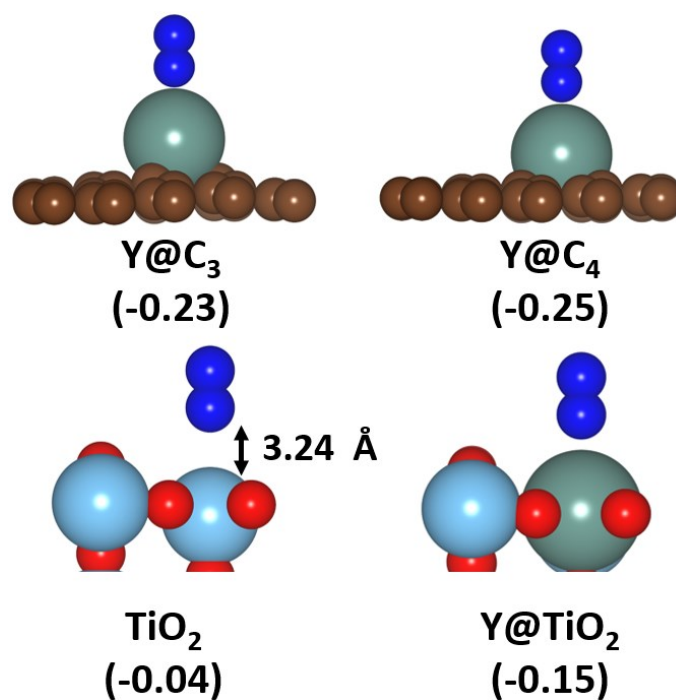


Fig. S15 The optimized geometries of adsorbed N_2 on Y@C_3 , Y@C_4 , $\text{TiO}_2(110)$ and Y@TiO_2 . The adsorption energy of N_2 at each site is listed in parenthesis (ΔE in eV). Green, sky blue, brown red, and blue balls indicate Y, Ti, C, O, and N atoms, respectively.

Table S1 Comparison of the as-synthesized Y-TiO₂-C and previously reported TiO₂-based materials and metal electrocatalysts for NRR.

Catalyst	Electrolyte	NH_3 yield rate	NH_3 FE	Ref.
1.7%Y-TiO ₂ -C	0.1 M HCl	$6.3 \mu\text{g h}^{-1} \text{mg}_{\text{cat.}}^{-1}$	11.2%@-0.22 V (vs. RHE)	This work
Boron-doped TiO ₂	0.1 M Na ₂ SO ₄	$14.4 \mu\text{g h}^{-1} \text{mg}_{\text{cat.}}^{-1}$	3.4%@-0.8 V (vs. RHE)	19
TiO ₂ /Ti	0.1 M Na ₂ SO ₄	$9.16 \times 10^{-11} \text{mol s}^{-1} \text{cm}^{-2}$	2.5%@-0.7 V (vs. RHE)	20
C-doped TiO ₂	0.1 M Na ₂ SO ₄	$16.22 \mu\text{g h}^{-1} \text{mg}_{\text{cat.}}^{-1}$	1.84%@-0.7 V (vs. RHE)	21

TiO ₂ /Ti ₃ C ₂ T _x	0.1 M HCl	26.32 μg h ⁻¹ mg _{cat.} ⁻¹	8.42%@-0.6 V (vs. RHE)	22
TiC/C	0.1 M HCl	14.1 μg h ⁻¹ mg _{cat.} ⁻¹	5.8%@-0.5 V (vs. RHE)	23
Ti ₃ C ₂ T _x (T = F, OH)	0.1 M HCl	20 μg h ⁻¹ mg _{cat.} ⁻¹	9.3%@-0.4 V (vs. RHE)	24
MXene	0.5 M Li ₂ SO ₄ (pH 2)	4.72 μg h ⁻¹ cm ⁻²	5.78%@-0.2 V (vs. RHE)	25
Ti ₃ C ₂ T _x				
<i>d</i> -TiO ₂ /TM	0.1 M HCl	1.24 x 10 ⁻¹⁰ mol s ⁻¹ cm ⁻²	9.17%@-0.15 V (vs. RHE)	26
TiO ₂ (V ₀)	0.1 M HCl	3.0 μg h ⁻¹ mg _{cat.} ⁻¹	6.5%@-0.12 V (vs. RHE)	8
Fe ₃ O ₄ /Ti	0.1 M Na ₂ SO ₄	5.6 x 10 ⁻¹¹ mol s ⁻¹ cm ⁻²	2.6%@-0.4 V (vs. RHE)	27
Bi nanosheets	0.1 M Na ₂ SO ₄	13.23 μg h ⁻¹ cm ⁻²	10.46%@-0.8 V (vs. RHE)	28
MoS ₂ /CC	0.1 M Na ₂ SO ₄	8.08 x 10 ⁻¹¹ mol s ⁻¹ cm ⁻²	1.17%@-0.5 V (vs. RHE)	29
Cr ₂ O ₃ microspheres	0.1 M Na ₂ SO ₄	25.3 μg h ⁻¹ mg _{cat.} ⁻¹	6.78%@-0.9 V (vs. RHE)	30
WO _{3-x} (V ₀)	0.1 M HCl	4.2 μg h ⁻¹ mg _{cat.} ⁻¹	6.8%@-0.9 V (vs. RHE)	31
γ-Fe ₂ O ₃	0.1 M KOH	0.212 μg h ⁻¹ mg _{cat.} ⁻¹	1.9%@0.0 V (vs. RHE)	32
Fe ₂ O ₃ -CNT	0.1 M KHCO ₃	0.22 μg h ⁻¹ mg _{cat.} ⁻¹	0.03%@-2.00 V (vs. RHE)	33

Pd _{0.2} Cu _{0.8} /rGO	0.1 M KOH	2.8 μg h ⁻¹ mg _{cat.} ⁻¹	0.4%@-0.2 V (vs. RHE)	34
β-FeOOH	0.5 M LiClO ₄	23.32 μg h ⁻¹ mg _{cat.} ⁻¹	4.5%@-0.75 V (vs. RHE)	35
TiO ₂ -rGO	0.1 M Na ₂ SO ₄	15.13 μg h ⁻¹ mg _{cat.} ⁻¹	3.3%@-0.9 V (vs. RHE)	36
Mn ₃ O ₄	0.1 M Na ₂ SO ₄	11.6 μg h ⁻¹ mg _{cat.} ⁻¹	3%@-0.9 V (vs. RHE)	37
CoS ₂ /NS-G	0.05 M H ₂ SO ₄	25 μg h ⁻¹ mg _{cat.} ⁻¹	7.8%@-0.9 V (vs. RHE)	38

References

1. Z. Di, Z. Linghong, R.E. Ruther, R.J. Hamers, *Nat. Mater.*, 2013, **12**, 836–841.
2. L. Zhang, L. X. Ding, G. F. Chen, X. Yang and H. Wang, *Angew. Chem. Int. Ed.*, 2019, **131**, 2638–2642.
3. G. W. Watt and J. D. Chrisp, *Anal. Chem.*, 1952, **24**, 2006–2008.
4. E. Skulason, T. Bligaard, S. Gudmundsdóttir, F. Studt, J. Rossmeisl, F. Abild-Pedersen, T. Vegge, H. Jonsson and J. K. Nørskov, *Phys. Chem. Chem. Phys.*, 2012, **14**, 1235–1245.
5. J. H. Montoya, C. Tsai, A. Vojvodic and J. K. Nørskov, *ChemSusChem*, 2015, **8**, 2180–2186.
6. J. G. Howalt and T. Vegge, *Phys. Chem. Chem. Phys.*, 2013, **15**, 20957–20965.
7. Y. Abghoui, A. L. Garden, J. G. Howalt, T. Vegge and E. Skúlason, *ACS Catal.*, 2016, **6**, 635–646.
8. Z. Han, C. Choi, S. Hong, T. S. Wu, Y. L. Soo, Y. Jung, J. Qiu and Z. Sun, *Appl. Catal. B Environ.*, 2019, **257**, 117896.
9. A. R. B. Höskuldsson, Y. Abghoui, A. B. Gunnarsdóttir and E. Skúlason, *ACS Sustainable Chem. Eng.*, 2017, **5**, 10327–10333.

10. Y. Abghoui, S. B. Sigtryggsson and E. Skúlason, *ChemSusChem*, 2019, **12**, 4265–4273.
11. C. Choi, S. Back, N.-Y. Kim, J. Lim, Y.-H. Kim and Y. Jung, *ACS Catal.*, 2018, **8**, 7517–7525.
12. G. Kresse and D. Joubert, *Phys. Rev. B*, 1999, **59**, 1758-1775.
13. G. Kresse and J. Furthmüller, *Comput. Mater. Sci.*, 1996, **6**, 15–50.
14. P. E. Blöchl, *Phys. Rev. B*, 1994, **50**, 17953–17979.
15. B. Hammer, L. B. Hansen and J. K. Nørskov, *Phys. Rev. B*, 1999, **59**, 7413–7421.
16. J. P. Perdew, K. Burke and M. Ernzerhof, *Phys. Rev. Lett.*, 1996, **77**, 3865–3868.
17. H. J. Monkhorst and J. D. Pack, *Phys. Rev. B*, 1976, **13**, 5188–5192.
18. J. K. Nørskov, J. Rossmeisl, A. Logadottir, L. Lindqvist, J. R. Kitchin, T. Bligaard and H. Jonsson, *J. Phys. Chem. B*, 2004, **108**, 17886–17892.
19. Y. Wang, K. Jia, Q. Pan, Y. Xu, Q. Liu, G. Cui, X. Guo and X. Sun, *ACS Sustainable Chem. Eng.*, 2018, **7**, 117–122.
20. R. Zhang, X. Ren, X. Shi, F. Xie, B. Zhang, X. Guo and X. Sun, *ACS Appl. Mater. Interfaces.*, 2018, **10**, 28251–28255.
21. K. Jia, Y. Wang, Q. Pan, B. Zhong, Y. Luo, G. Cui, X. Guo and X. Sun, *Nanoscale Adv.*, 2019, **1**, 961–964.
22. J. Zhang, L. Yang, H. Wang, G. Zhu, H. Wen, H. Feng, X. Sun, X. Guang, J. Wen and Y. Yao, *Inorg. Chem.*, 2019, **58**, 5414–5418.
23. G. Yu, H. Guo, W. Kong, T. Wang, Y. Luo, X. Shi, A. Asiri, T. Li and X. Sun, *J. Mater. Chem. A*, 2019, **7**, 19657.
24. J. Zhao, L. Zhang., X. Xie, X. Li, Y. Ma, Q. Liu, W. Fang, X. Shi, G. Cui and X. Sun, *J. Mater. Chem. A*, 2018, **6**, 24031–24035.
25. Y. Luo, G. Chen, L. Ding, X. Chen, L. Ding and H. Wang, *Joule*, 2019, **3**, 279–289.
26. L. Yang, T. Wu, R. Zhang, H. Zhou, L. Xia, X. Shi, H. Zheng, Y. Zhang and X. Sun, *Nanoscale*, 2019, **11**, 1555–1562.
27. Q. Liu, X. Zhang, B. Zhang, Y. Luo, G. Cui, F. Xie and X. Sun, *Nanoscale*, 2018, **10**, 14386–14389.

28. L. Li, C. Tang, B. Xia, H. Jin, Y. Zheng and S. Qiao, *ACS Catal.*, 2019, **9**, 2902–2908.
29. L. Zhang, X. Ji, X. Ren, Y. Ma, X. Shi, Z. Tian, A. M. Asiri, L. Chen, B. Tang and X. Sun, *Adv. Mater.*, 2018, **30**, 1800191.
30. Y. Zhang, W. Qiu, Y. Ma, Y. Luo, Z. Tian, G. Cui, F. Xie, L. Chen, T. Li and X. Sun, *ACS Catal.*, 2018, **8**, 8540–8544.
31. Z. Sun, R. Huo, C. Choi, S. Hong, T.-S. Wu, J. Qiu, C. Yan, Z. Han, Y. Liu and Y.-L. Soo, *Nano Energy*, 2019, **62**, 869–875.
32. J. Kong, A. Lim, C. Yoon, J.H. Jang, H.C. Ham, J. Han, S. Nam, D. Kim, Y.E. Sung, J. Choi and H.S. Park, *ACS Sustainable Chem. Eng.*, 2017, **5**, 10986–10995.
33. S. Chen, S. Perathoner, C. Ampelli, C. Mebrahtu, D. Su and G. Centi, *Angew. Chem. Int. Ed.*, 2017, **56**, 2699–2703.
34. M. M. Shi, D. Bao, S. J. Li, B. R. Wulan, J. M. Yan and Q. Jiang, *Adv. Energy Mater.*, 2018, **8**, 1800124.
35. X. Zhu, Z. Liu, Q. Liu, Y. Luo, X. Shi, A. M. Asiri, Y. Wu and X. Sun, *Chem. Commun.*, 2018, **54**, 11332.
36. X. Zhang, Q. Liu, X. Shi, A. M. Asiri, Y. Luo, X. Sun and T. Li, *J. Mater. Chem. A*, 2018, **6**, 17303.
37. X. Wu, L. Xia, Y. Wang, W. Lu, Q. Liu, X. Shi and X. Sun, *Small*, 2018, **14**, 1803111.
38. P. Chen, N. Zhang, S. Wang, T. Zhou, Y. Tong, C. Ao, W. Yan, L. Zhang, W. Chu, C. Wu and Y. Xie, *PNAS*, 2019, **116**, 6635–6640.